18

Identification of NV Centers in Synthetic Fluorescent Nanodiamonds and Control of Defectiveness of Crystallites Using Electron Paramagnetic Resonance

© V.Yu. Osipov[1,2], K.V. Bogdanov[2], F. Treussart[3], A. Rampersaud[4], A.V. Baranov[2]

[1] Ioffe Institute,
194021 St. Petersburg,
[2] ITMO University,
197101 St. Petersburg,
[3] Université Paris-Saclay, CNRS, ENS Paris-Saclay, CentraleSupélec, LuMIn,
91190, Gif-sur-Yvette, France
[4] Columbus Nanoworks, Columbus,
43212 Ohio, United States
e-mail: osipov@mail.ioffe.ru, kirw.bog@gmail.com

Received October 29, 2021
Revised November 26, 2021
Accepted November 07, 2021

A 100 nm synthetic diamond particle with a large (> 4 ppm) amount of nitrogen vacancy (NV) centers has been studied. The latter exhibit lines associated with forbidden $\Delta m_s = 2$ and allowed $\Delta m_s = 1$ transitions in the electron paramagnetic resonance (EPR) spectra of the ground state of the $NV^{(-)}$ center. The luminescence intensity of particles in the range $550-800$ nm increases with an increase in the irradiation dose of 5 MeV electrons and correlates with the integrated intensity of the peak EPR line with a g-factor $g = 4.27$. This value is used to estimate the concentration of $NV^{(-)}$ centers and to select diamond powders with the highest fluorescence intensity. The dependence of the EPR signal intensity of the $\Delta m_s = 2$ transition of the $NV^{(-)}$ center on the microwave power that increases before decaying rather well characterizes the crystal quality of the local environment of the centers under study in these particles. The intensity of the $x, y\Delta m_s = 1$ transition (at ~ 281.2 mT, 9.444 GHz) turns out to be sensitive to changes in particle size in the submicron range and the appearance of near-surface defects obtained during mechanical processing.

Keywords: luminescence, nitrogen vacancy centers, synthetic diamond, nanocrystals, electron paramagnetic resonance.

DOI: 10.21883/EOS.2022.02.53968.2872-21

Introduction

Fluorescent micro- and nanodiamonds with nitrogen-vacansion (NV) centers are a new promising engineering material for innovative information applications in telecommunications, nanophotonics and biomedicine [1–4]. Potential applications of these materials require further development of *non-optical* diagnostic tools for the centers responsible for luminescence in these materials.

In synthetic nanodiamonds of size range $100-130$ nm, signatures of $NV^{(-)}$ triplet centers (the so-called W15 centers) [5,6] have been detected and identified recently, by electron paramagnetic resonance (EPR). The W15 center was observed for the first time about 40 years ago in bulk diamond crystals irradiated with electrons or protons, containing nitrogen impurities [7]. Due to the peculiarities of its microscopic structure, the $NV^{(-)}$ center has spin $S = 1$ and is optically active, yielding a photoluminescence characterized by a zero-phonon line at 638 nm [8,9]. Specific EPR signals corresponding to $NV^{(-)}$ centers are due to the so-called forbidden ($\Delta m_s = 2$)[1] transitions between the Zeeman-splitted energy levels of the $S = 1$ triplet state of the center in the magnetic field [10]. The study of the luminescence of these centers in nano- and microparticles is an essential task in connection with the possible applications of the radiation of $NV^{(-)}$ centers in nanophotonics, optical secure communication channels, and biomedical research at the cellular level. In this article, we study $NV^{(-)}$ centers in 100 nm fluorescent particles ground from microcrystals of synthetic HPHT Ib diamond and subsequently irradiated with a high-energy electron beam, and finally annealed. The results of these studies, performed by optical and EPR methods, are compared with each other. The surface and near-surface layers of nanoparticles up to $5-10$ nm thick are sources of many of defects (with a two-dimensional density of $\sim 0.2-1\text{nm}^{-2}$), both point defects, and cooperative defects, formed there as a result of split of the crystal lattice during mechanical grinding and of the impact of large shear and tensile stresses elements on the near-surface layers

[1] Here Δm_s corresponds to change in the projection of the spin magnetic moment $S = 1$ per direction of the magnetic field, i.e. change in the magnetic quantum number of the electronic state.

consecutive from grinding [11,12]. The problem of a mechanically disturbed layer in diamond particles has recently been considered in the context of the electron density shift from donor nitrogen to centers within the damaged layer, leading to formation of nonparamagnetic nitrogen with zero magnetic moment [13]. Surface centers can also change the charge state of optical centers and paramagnetic defects inside nanoparticles, and „exclude“ some of them from the analyzed phenomenon or process. As the particle diameter decreases, the role of surface defects and defects located in a mechanically damaged layer increases. As the size of diamond particles decreases, starting approximately from sizes in the 150−200 nm range, the properties of the crystals begin to change. Thus, the width of the Raman line of diamond in nanoparticles with average size of 75−100 nm is increased by $2.0-2.7\,\mathrm{cm}^{-1}$ compared to this value in a bulk diamond crystal, from which they were derived. In particles obtained by grinding with average size of 25 nm, the Raman line of diamond broadens even more — by $3.9\,\mathrm{cm}^{-1}$ [14]. Such a trend, which manifests itself in large additional broadenings ($\sim 4\mathrm{cm}^{-1}$) of the diamond Raman line at small particle sizes, and, accordingly, in insignificant line broadenings ($< 1\,\mathrm{cm}^{-1}$) at large sizes (~ 180 nm), means that the optical properties of particles associated with the phonon subsystem begin to differ from the bulk parameters even at sizes of ≤ 400 nm. An important role in this is played by collective disturbances in the crystal lattice organized on a large scale (from 30−50 nm and above). Among them are dislocations, polyvacancies, nanopores, regions with high mechanical stresses, etc. The influence of mechanical stresses on the structure of electronic levels of $NV^{(-)}$ centers in diamond and nanostructures based on it was reported in [15,16]. Therefore, one could expect that defects and cracks induced in the near-surface layer of crystals by grinding would change the parameters of the electronic levels of some nearby $NV^{(-)}$ centers due to the mechanical stresses they create in the diamond particles lattice with size of ≤ 100 nm. The main distinguishing feature of this article is that in order to analyze the crystal quality of the diamond lattice in the nearest surrounding[2] from the $NV^{(-)}$ centers, we recorded the characteristic curves of EPR signal saturation of these centers depending on the absorbed microwave power. This makes it possible to qualitatively estimate the effect of defects and paramagnetic centers, located on the nanoparticles surface, on $NV^{(-)}$ centers located randomly uniformly within the nanoparticle, and to estimate under what conditions the surface begins to strongly modify the characteristics of $NV^{(-)}$ centers in the lattice due to radiative recombination in the optical or microwave ranges. Previously, this technique was successfully tested and applied to study the crystalline quality of submicron (< 1000 nm) diamonds obtained by sintering at high pressures and temperatures from 5 nm detonation-synthesized nanodiamond [17]. In this case, the EPR signal of the main paramagnetic center P1, associated with substituting nitrogen impurities in the diamond lattice and having a spin $S = 1/2$ [18], was selected for monitoring.

Samples and study methods

Fluorescent nanodiamond (FND) particles with average size of 100 nm were obtained from synthetic (with atomic nitrogen impurities) microcrystalline HPHT Ib diamond with grain size of up to 150 μm. The microdiamonds were first subjected to intensive crushing and grinding, and then the submicron fraction separated from the grinding (average size 104 nm, particle distribution function width at half maximum of ~ 76 nm) was irradiated in a layer several millimeters thick with a high-energy electron beam (5 MeV) and annealed in inert atmosphere at 800°C. The fraction with nominal value of 100 nm was selected by centrifugation in aqueous medium. Electron beam irradiation was used to create vacancies in the diamond lattice, and subsequent annealing served to ensure mobility of vacancies in the lattice and their capture by isolated nitrogen impurities as a result of random walk. The impurity nitrogen concentration in the original HPHT Ib microcrystals was 150 ± 10 ppm. The electron current density in the high-energy beam was $32\,\mu\mathrm{A/cm}^2$. During irradiation, the powdered material was cooled using a special device to prevent parasitic overheating. The material irradiated with electrons during the integral periods of 16, 32 and 40 h is designated as FND-1, FND-2, FND-3. These exposures were obtained by one, two, or three successive exposure sessions lasting 16 and 8 h. Long irradiation exposures of 100 nm particles were selected to increase the number of induced vacancies and, consequently, $NV^{(-)}$ centers in the resulting material. Basically, submicron (~ 100 nm) particles have no significant disadvantages[3] for the process of creating vacancies and NV centers in diamond compared to micrometer-sized and larger crystals. This results from the fact that the probability of formation of one NV center by a vacancy in an individual single-crystal particle with average nitrogen impurity level asymptotically tends to 1 with an increase in the crystal grain size (L_c) at $L_c > 40-50$ nm and the dependence on L_c is weak in this range [19]. The minimum nominal exposure dose corresponding to the lowest exposure duration was $7 \cdot 10^{18}\,\mathrm{cm}^{-2}$. Taking into account the different cooling conditions of the powders in the first and subsequent irradiation sessions, the equivalent exposure dose led to different amounts of optical centers induced in the material due to overheating. The samples that passed the irradiation and annealing steps were then subjected to intensive chemical purification in boiling acids in order to remove parasitic metal impurities, mainly iron-containing complexes. The samples were manufactured

[2] On the order of the phonon coherence length in the diamond lattice at room temperature or the average distance between $NV^{(-)}$ centers and other paramagnetic defects, depending on the situation, also including temperature.

[3] The disadvantages of submicron diamond powder include the worst thermal conductivity and increased volatility compared to micron-sized crystallite powders.

and processed by Columbus Nanoworks, Inc. (Columbus, Ohio, USA).

The EPR spectra of the samples were recorded at room temperature using a JEOL JES-FA 300 EPR spectrometer (Japan) at a frequency of 9.5 GHz. EPR signals spectra with g-factors within the range of 4.00–4.30 were recorded at a low power of microwave radiation of 0.003 mW, modulation amplitude of 0.2 mT, modulating magnetic field frequency of 100 kHz, number of signal accumulations of 10–16. The time constant was 0.03 s, the total spectrum recording time for one pass was 120 s for the magnetic field scan interval 130–200 mT. At low microwave powers ($P_{\mathrm{MW}} < 0.01$ mW), there were no distortions in the waveform of the EPR signals that could indicate saturation, and the signal growth with increasing P_{MW} was almost proportional to $\sqrt{P_{\mathrm{MW}}}$. The concentrations of $NV^{(-)}$ centers were estimated by double integration of the EPR signal ($g = 4.27$) taken at low microwave power ($P_{\mathrm{MW}} \approx 0.003$ mW), and referring the obtained value to the weight of the powdered sample. To obtain the absolute value of the concentration of $NV^{(-)}$ centers in units of „ppm" standards with known concentration of paramagnetic centers $S = 1$ and $S = 1/2$ were used as a reference for comparison [10,20] and the technique described in [10] was used. At microwave powers above 0.03 mW, a deviation from linearity was noted for the dependence of EPR signal ($g_1 = 4.27$) peak intensity (Ipp)4 on the square root of the microwave power $\sqrt{P_{\mathrm{MW}}}$. Here we neglect the strong asymmetry of the EPR line ($g_1 = 4.27$), of the EPR signal ($g_1 = 4.27$) from the root of the microwave power $\sqrt{P_{\mathrm{MW}}}$. To build saturation curves for the peak intensity of the EPR signal I_{pp} ($g_1 = 4.27$) based on ($\sqrt{P_{\mathrm{MW}}}$), the EPR spectra were additionally recorded for a number of values of P_{MW} within the range from 0 to 200 mW for samples FND-1, FND-2 and micron-sized HPHT Ib diamond crystals with $NV^{(-)}$ centers. In order to better match and compare trends I_{pp} ($\sqrt{P_{\mathrm{MW}}}$) at large values of P_{MW}, the saturation curves for different samples were normalized by the value of I_{pp} ($P_{\mathrm{MW}} = 0.003$ mW): I_{pp} (P_{MW}/I_{pp} ($P_{\mathrm{MW}} = 0.003$ mW).

For simultaneous comparison and analysis of EPR signals from forbidden ($\Delta m_s = 2$) and allowed ($x, y\ \Delta m_s = 1$) transitions in $NV^{(-)}$ centers of different samples, we additionally recorded EPR spectra within a wide range of magnetic fields from 120 to 320 mT and plotted the dependence of the ratio of the peak intensities of both signals $I_{pp}^{\mathrm{all}}/I_{pp}^{\mathrm{forb}}$ as a function of $\sqrt{P_{\mathrm{MW}}}$. The indicated spectra were taken with the same shooting parameters stated above.

The luminescence spectra were measured using an inVia micro-Raman unit (Renishaw, UK) using exciting laser radiation at wavelength of 532 nm and a $50^{\times}$ microscope objective focusing the radiation into a spot with a diameter of $\sim 2\,\mu$m on the sample surface. Luminescent radiation was collected in backscattering geometry from the sample surface. Fluorescence images of particles deposited from a drop of aqueous suspension were obtained using a Nikon Eclipse TiS inverted epifluorescence inverted microscope with the use of a Texas Red Cube optical filter (excitation 540–580 nm, transmitted radiation 600–660 nm). The images were obtained at 10 ms exposure using a $10^{\times}$ microscope objective. Optical and fluorescent images of isolated FND particles were also obtained using a multifunctional video microscope of our own design based on an inverted Nikon Eclipse Ti-E, operating in two modes: differential interference contrast (DIC) and total internal reflection fluorescence microscopy (TIRF). In the DIC mode, transmitted white light from a halogen lamp (OSRAM HLX 64623) was used, and the image contrast was selected by adding a small angle between the polarizer and analyzer in the operating circuit. In the TIRF configuration, we used 561 nm excitation radiation from a continuous-wave solid-state laser (SLIM-561-100, Oxxius S.A., Lannion, France), a dichroic beam splitter with constant 97% transmission above the edge at 561 nm (zt561rdc, Chroma Corporation, USA) and a bandpass filter (FF01-697/75, Semrock, USA), which transmits radiation in a $\sim$ 75 nm wide band centered on 697 nm. The power of the laser beam, measured before entering the optical system of the microscope, was $\sim$ 8–10 mW. In both cases, a $100^{\times}$ immersion microscope objective (CFI Apo TIRF $100^{\times}$, NA = 1.49, Oil, Nikon, Japan) was used. The particles were deposited by dropcasting a microdroplet of diamond suspension on a rotating coverglass with thickness of $\sim 170\mu$m (80 s, 2000 rpm/s, SPIN150 device, APT GmbH, Germany), preliminarily processed in oxygen plasma in a Femto device 40 KHz (Diener/Femto Plasma Cleaner, Germany) for 10 min at pressure of 0.5 mbar. The EMCCD camera (iXon-DU885, Andor Technology) used for image acquisition was cooled to -79.8°C. Sizes of the registered images were $\sim 80 \times 80\,\mu$m (1004 × 1002 pixels). The size of one pixel in the sample plane was $\sim$ 80 nm.

Experimental results and discussion

Electron paramagnetic resonance

$NV^{(-)}$ centers located in the volume of diamond particles and multivacancies, usually appearing on the surface of particles subjected to grinding and/or other mechanical damage, are triplet centers with spin $S = 1$. The spin Hamiltonian of the $NV^{(-)}$ center in magnetic field $\mathbf{B}$ (B_x, B_y, B_z) has the following form [21,22]:

$$H = \hat{g}\mu_{\mathrm{B}}\mathbf{B}\cdot\mathbf{S} + D\left[S_z^2 - \frac{1}{3}S(S+1)\right] + E(S_x^2 - S_y^2), \quad (1)$$

Here $\mathbf{S}$ is the spin operator, S_z is the operator associated with the z-component of $\mathbf{S}$ given by the symmetry axis of the NV center, i.e. direction $\langle 111\rangle$ in the crystal lattice, S_x, S_y is the spin-1 projection operators on the coordinate axes x and y, $\hat{g} is the g$-tensor (or g-factor of electron spin $g_{xx} = g_{yy} = g_{zz} = 2.0028 pm 0.0003$), D is the fine structure parameter, associated with the level splitting in

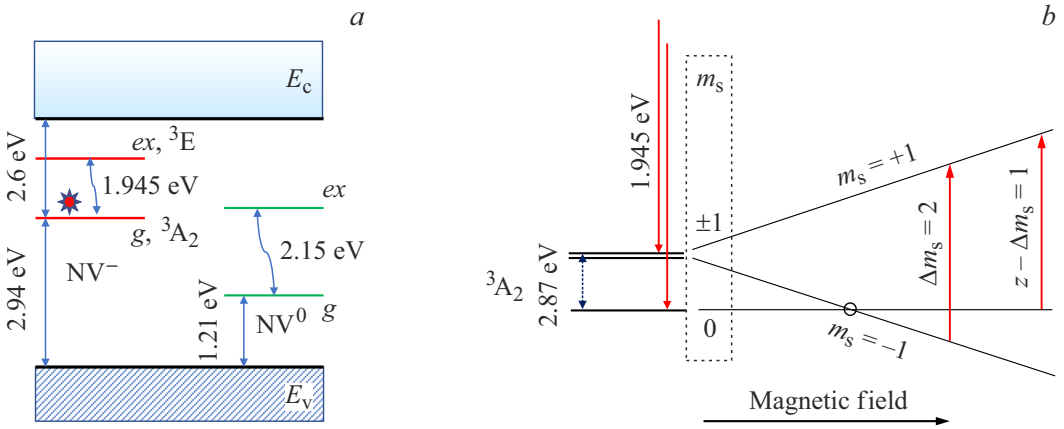

Figure 1. Diagram of the main energy levels of the $NV^{(0)}$ and NV centers in the band gap of diamond (*a*) and the Zeeman splitting of the ground state levels of the $^3A_2$ $NV^{(-)}$ center in magnetic field (*b*). Designations: *g* — ground state, *ex* — excited state, E_c — conduction band edge, E_v — valence-band edge, m_s — magnetic quantum number of the energy level in the triplet center.

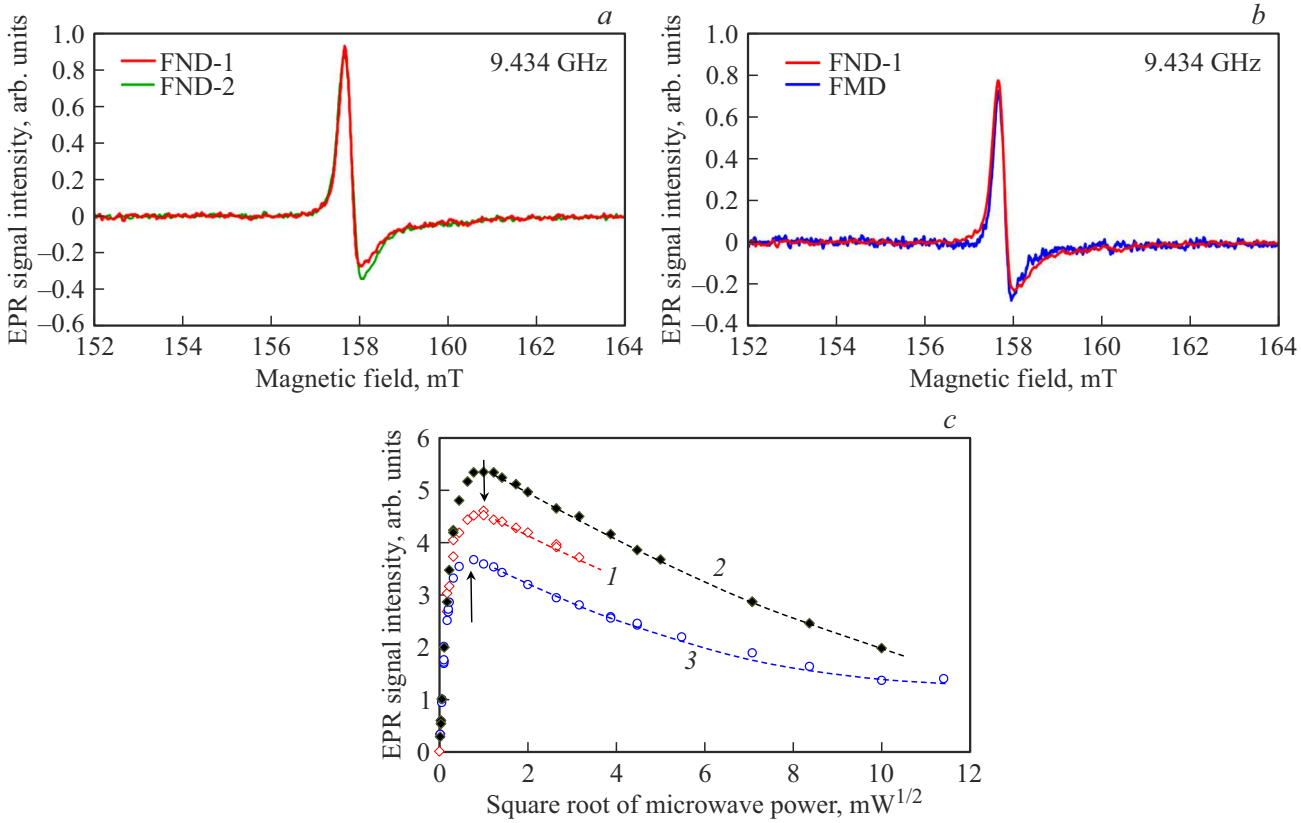

Figure 2. EPR spectra of fluorescent synthetic HPHT Ib diamond (FND-1, FND-2, and FMD) in comparison pairs FND-1/FND-2 (*a*) and FND-1/FMD (*b*) and saturation curves of the peak intensity of the EPR signal ($g_1 = 4.27$) versus the square root of the microwave power within the range from 0 to 140 mW (*c*) for samples FND-1 (*1*), FND-2 (*2*) and reference HPHT Ib diamond microcrystals with $NV^{(-)}$ centers (*3*). Microwave frequency is ≈ 9.43 GHz. For better comparison, all saturation curves are normalized to microwave power $P_{MW} = 0.003$ mW.

zero magnetic field (singlet-triplet gap), *E* is the parameter associated with the splitting induced by stresses in the crystal lattice, μ_B is the Bohr magneton. In fact, the *D* parameter also depends on stresses, including thermally induced stresses in the lattice [1,15,21]. The spin-Hamiltonian in formula (1) is approximate and does not take into account hyperfine and quadrupole interactions, in particular, interactions of electron spins of $NV^{(-)}$ centers with nuclear magnetic moments ^{14}N (and ^{13}C), the Zeeman term for the nuclear magnetic moment of the nitrogen atom ^{14}N

($I = 1$), and the term associated with the quadrupole nuclear interaction. $NV^{(-)}$ centers are triplet in both the ground unexcited ($^3A_2$) and optically excited (^3E) states. Both systems of levels are within the diamond band gap (Fig. 1) [23,24]. Then, in the context of EPR studies, we will consider only the main optically unexcited states of triplet centers (Fig. 1, *b*). The positions of EPR lines corresponding to forbidden ($\Delta m_s = 2$) and allowed ($\Delta m_s = 1$) transitions between these states at the selected microwave range is set on the magnetic field scale by the unique parameters of the spin-Hamiltonians of these centers. The latter take into account the exchange interaction between individual spins at the centers, while the parameter D of the spin Hamiltonian, which sets the width of the gap between the levels $|^3A_2, 0\rangle$ and $|^3A_2, 1\rangle$ of the center in zero magnetic field is usually inversely proportional to the third power of the distance between individual spins 1/2 at a composite triplet center [7,25]. Here, the entries $0\rangle$ and $\pm1\rangle$ denote the states with antiparallel ($m_s = 0$) and parallel ($m_s = \pm1$) orientations of individual spins 1/2 at the triplet center, respectively. Index 3 means triplet structure. The parameter D of the spin Hamiltonian of the $NV^{(-)}$ center was determined in the late 1970s based on the analysis of the lines positions in the EPR spectrum of the center [7], and then repeatedly refined [26]. It is equal to $D = 954 \cdot 10^{-4}\,\text{cm}^{-1}$ with 0.3% precision [7]. This value approximately corresponds to the distance of 0.3 nm between individual spins (unpaired orbitals) $S = 1/2$ at the triplet center. The width of the corresponding gap is 2.87 GHz (or 12 eV). The ratio E/D in a number of practical cases is about 0.002–0.003 or even much less. The temperature dependence of $D(T)$ is weak linear with a slope coefficient of about -75 kHz/K in the vicinity of room temperature.

The $|^3A_2, 0\rangle$ and $|^3A_2, 1\rangle$ levels are also ground states for radiative optical transitions ($h\nu = 1.945$ eV) coming from the optically excited states levels $|^3E, 0\rangle$ and $|^3E, 1\rangle$, which also have a triplet structure.

The EPR spectra of samples FND-1 and FND-2, which differ in the irradiation dose of high-energy electrons, are shown in Fig. 2, *a, b* within the range of magnetic fields from 152 to 164 mT. In the domain of[4] in magnetic field and at microwave powers up to 1 mW in the spectra there is only one characteristic narrow line $g_1 = 4.27$ associated to $NV^{(-)}$ centers, the intensity of which increases with the irradiation dose. The signals from other triplet centers, for example, multivacancies, are practically absent even in a range extended by 20 mT (Fig. 2, *a, b*).[5] This means that diamond microcrystals grinding to 100 nm level does not yet quantitatively lead to appearance of a significant number of surface defects (multivacancies and dangling bonds) i.e. defects that could appear during mechanical

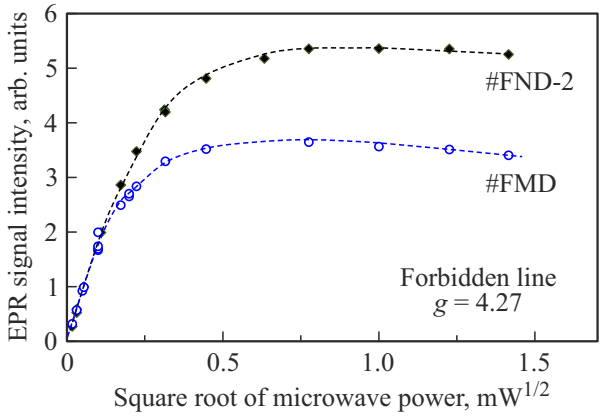

Figure 3. Saturation curves of the peak intensity of the EPR signal ($g_1 = 4.27$) versus the square root of the microwave power within the range from 0 to 2 mW for the FND-2 (black diamonds) and FMD (blue circles) samples. Curves are normalized at power $P_{MW} = 0.003$ mW.

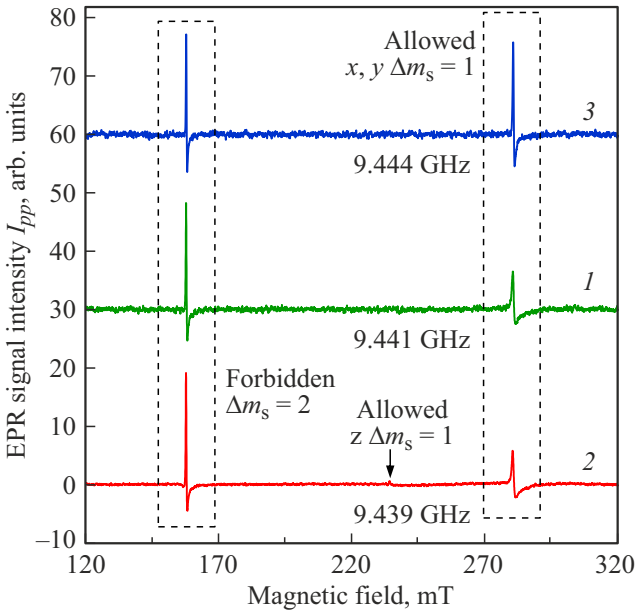

Figure 4. The EPR spectra of FND-1 (*1*), FND-2 (*2*) and FMD (*3*) in a wide range of magnetic fields (from 120 to 320 mT), demonstrating forbidden ($\Delta m_s = 2$) and low-field allowed ($x, y\ \Delta m_s = 1$) microwave transitions between triplet states $|^3A_2, -1\rangle$, $|^3A_2, +1\rangle$ and $|^3A_2, 0\rangle$ and $|^3A_2, +1\rangle$. For better comparison, all spectra are normalized to the peak amplitude of the EPR signal with g-factor $g = 4.27$. Microwave frequency is ≈ 9.44 GHz. The upper limit of the range lies 16 mT below the position of the intense EPR signal from paramagnetic nitrogen defects (P1) in diamond with a characteristic hyperfine structure.

[4] This refers to the range of magnetic fields where weak EPR signals with g-factor $g \approx 4$ are located. The specificity of the studied samples is such that parasitic signals from iron-containing complexes (with g-factor $g = 4.25$–4.27), also located in this range, are absent after chemical cleaning.

[5] Multivacancies, linear clusters of small extent, consisting of vacancies, cause the presence of the EPR signal with a g-factor $g_2 = 4.00$ magnetic field range of about ~ 10 mT from the EPR signal corresponding to $NV^{(-)}$ centers. Like the latter, they are triplet centers. For example, they are present in polycrystalline nanodiamonds of dynamic synthesis with average size within the range of 25–1000 nm.

processing of microcrystals and and could quench the luminescence of $NV^{(-)}$ centers inside 100 nm particles due to the mechanism of optical excitation migration from $NV^{(-)}$ to the defective surface. The EPR signal from $NV^{(-)}$ centers in nanoparticle powder samples has asymmetric, non-Lorentz line shape, which is due to the type of center symmetry in the crystal, the features of the parameters D and E of the spin Hamiltonian of the center, and to some extent, their dependence on local mechanical stresses in the crystal lattice. Note that in HPHT Ib diamond nanoparticles not subjected to electron irradiation, the EPR signal with the g factor $g_1 = 4.27$ (from $NV^{(-)}$ centers) is absent. As the microwave power P_{MW} increases above 0.4 mW, the peak signal intensity $g_1 = 4.27$ for both FND-1 and FND-2 samples saturates, and at powers above 2–3 mW it exhibits already monotonous slow decreases extending up to the values of $P_{MW} \sim 100$ mW (Fig. 2, *c*, curves *1* and *2*). In this case, the width ΔH_{pp} of the $g_1 = 4.27$ line slightly (within 20%) increases from 0.49 to 0.59 mT within the interval P_{MW} from 0.001 to 100 mW. This points to the prevailing occupancy of the upper Zeeman split-off energy level $|^3A_2, +1\rangle$ implemented at these values P_{MW} (due to forbidden $\Delta m_s = 2$ transitions), to relatively long spin relaxation times (both spin-spin and spin-lattice) and, accordingly, to the high quality of the diamond crystal lattice in the nearest vicinity of $NV^{(-)}$ centers.[6] No attempts were made in this article to determine the exact spin-spin and spin-lattice relaxation times for $NV^{(-)}$ centers, rather than due to difficulties in correct data interpretation, but due to the fact that the shape of the saturation curve I_{pp} (P_{MW}) qualitatively characterizes the *crystalline quality of the local surrounding* of the centers under study quite well. Figure 2, *c* additionally shows the saturation curve of the peak intensity of the EPR signal $g_1 = 4.27$ for FMD fluorescent diamond microcrystals (with $NV^{(-)}$ centers) a few microns in size (curve *3*). The latter saturates at slightly lower (~ 0.2–0.3 mW) microwave powers than for 100 nm fluorescent diamond particles, which indicates a somewhat higher, but not fundamentally different, crystalline quality of HPHT Ib diamond microcrystals irradiated with high-energy electrons than that of 100 nm particles obtained by grinding from the same micron-sized crystals and subsequent irradiation. An earlier tendency to saturation of the EPR signal $g_1 = 4.27$ in the FMD sample (compared to FND-1, FND-2) is found already in the microwave power range of 0.03–0.2 mW, where 100 nm and micron samples with $NV^{(-)}$ centers show different deviations (strong and weak) from the linear dependence $I_{pp} \sim \sqrt{P_{MW}}$ at low powers (Fig. 3). Thus, paramagnetic and other lattice defects located on the surface of 100 nm particles do not yet have a strong effect on the spin-spin and spin-lattice relaxation times of the microwave-excited state $|^3A_2, +1>$ of $NV^{(-)}$ centers. This EPR technique can be used to assess the potential suitability of $NV^{(-)}$ centers as luminescence centers in specific submicron crystals, since the high crystal quality of the diamond lattice around the center contributes to appearance of both long spin and optical [7] relaxation times, and vice versa. Additionally, Figure 4 shows the EPR spectra of the studied samples FND-1, FND-2 and the reference microcrystalline sample FMD in a wide range of magnetic fields (from 120 to 320 mT). On all spectra near the upper boundary of this interval, there is a signal corresponding to the so-called allowed x, y $\Delta m_s = 1$ transition between the energy level of the $|^3A_2, 0\rangle$ with $m_s = 0$ not sensitive to magnetic field and one of the levels of the $NV^{(-)}$ center triplet state with $m_s = \pm 1$ undergoing a Zeeman shift towards higher energies. This signal, corresponding to a low-field x, y allowed transition within the microwave range, is located approximately at ~ 281 mT (at $\nu = 9.44$ GHz).

The spectra shown in Fig. 4 were measured at $P_{MW} = 1$ W, i.e. low power. With an increase in microwave power, the intensity of the EPR line x, y $\Delta m_s = 1$ (for samples FND-1, FND-2) reaches a maximum, saturates, and then decreases in intensity even faster than the intensity of the EPR line for the forbidden transition $\Delta m_s = 2$. At microwave powers above 7 mW, the first

[6] For example, in a detonation diamond containing $NV^{(-)}$ centers around ~ 1.2 ppm, the EPR signal $g_1 = 4.27$ does not saturate up to a microwave power of 200 mW due to large concentration of paramagnetic centers $S = 1/2$ (1300 ppm) and other non-magnetic defects in the crystal lattice, including those associated with the presence of nitrogen pairs (A-centers) in an amount up to 2 wt.%.

[7] Here we mean the case of optical pumping and relaxation of the optically excited state of the $NV^{(-)}$ center.

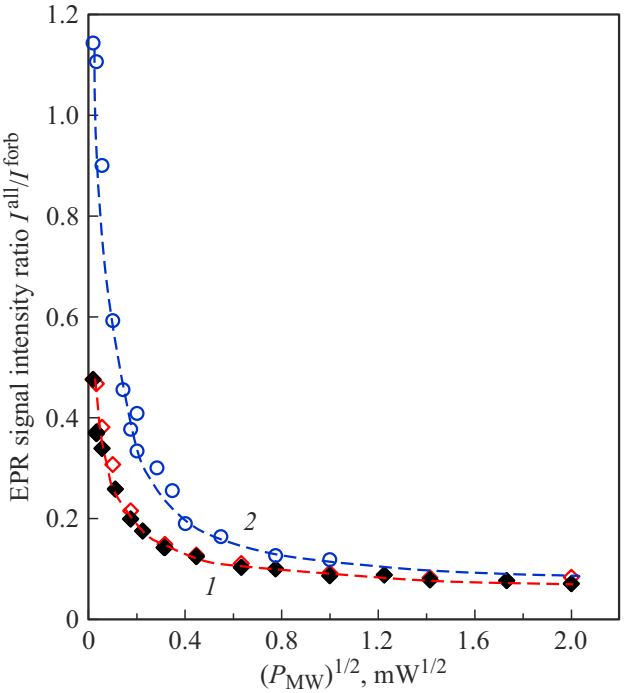

Figure 5. Ratio of peak intensities of EPR lines for allowed (x, y $\Delta m_s = 1$) and forbidden ($\Delta m_s = 2$) transitions (I_{all}/I_{forb}) depending on P_{MW} for samples FND-1 and FND-2 (black and red unfilled diamonds) and reference FMD HPHT Ib diamond microcrystals with $NV^{(-)}$ centers (blue empty circles).

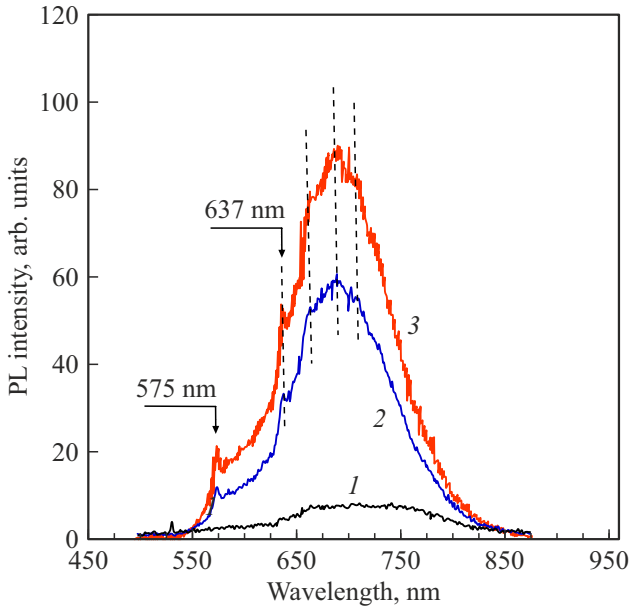

Figure 6. Luminescence spectra of 100 nm particles of synthetic HPHT Ib diamond with $NV^{(-)}$ centers for materials with different dose of high-energy electron beam irradiation (FND-1, FND-2, FND-3). The spectra were excited by laser radiation of 532 nm.

one becomes practically unobservable[8] in nanoparticles with size of 100 nm (due to broadening and decrease in peak amplitude), while the second one (forbidden transition line) is observed up to powers of the order of 160 mW. Figure 5 shows the ratio I_{all}/I_{forb} of the peak amplitudes of EPR lines for allowed (x, y $\Delta m_s = 1$) and forbidden ($\Delta m_s = 2$) transitions depending on P_{MW} for samples FND-1, FND-2 and FMD. It can be seen that the experimental points for FND-1 and FND-2 (black and red diamonds) practically coincide and lie on the same curve *1*. Moreover, as P_{MW} increases, the ratio I_{all}/I_{forb} (within the interval $P_{MW} = 0-1$ mW) decreases fast in both cases. At the same time, the I_{all}/I_{forb} ratio for the FMD HPHT Ib diamond microcrystals with $NV^{(-)}$ centers is characterized by large values in the $P_{MW} = 0-1$ mW range (blue circles, Fig. 5), which corresponds to the best observability of the signal from the allowed x, y $\Delta m_s = 1$ transition to FMD within this power range. In this case, the I_{all}/I_{forb} ratio decreases even faster (from 1.14 to 0.07) than for samples FND-1 and FND-2 within the power interval 0–4 mW (curve *2* in Fig. 5). This additionally points to the special sensitivity of the EPR line of the allowed (x, y $\Delta m_s = 1$) transition at the $NV^{(-)}$ center to defects and imperfections of the crystal lattice on the surface of nanoparticles. The effect of the latter is reduced to broadening of the allowed transition line and a decrease in its peak intensity. This effect is enhanced with decreasing particle size (down to 5–10 nm) to such an extent that allowed transitions are not observed

[8] In micron-sized crystals, the EPR signal from allowed $\Delta m_s = 1$ transitions in $NV^{(-)}$ centers is observed up to microwave powers of the order of 100 mW.

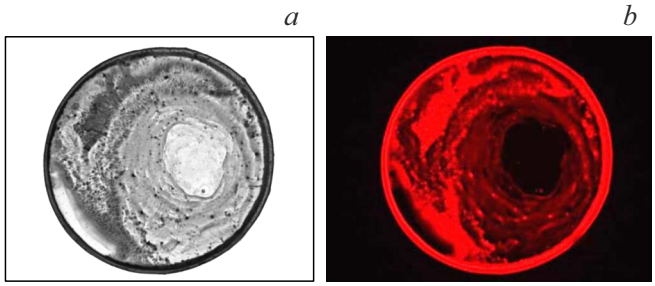

Figure 7. Optical image of a dried drop of aqueous suspension of synthetic diamond nanoparticles FND-3 (*a*) with $NV^{(-)}$ centers and the corresponding fluorescent image of the drop (*b* /), obtained using an epifluorescence microscope and illuminating laser with wavelength of 532 nm. The areas of intense red glow correspond to areas on the substrate where the highest concentration of deposited FND-3 particles occurs. Ring diameter is 0.8–0.9 mm.

at all in 5–10 nm particles [5,6]. Some broadening of the allowed transition line is apparently due to the local spread of the parameters of the spin Hamiltonian D, E over the ensemble of $NV^{(-)}$ centers in the material. The effect of mechanical stresses arising in crystallites on the values of the parameters of the spin Hamiltonians for the $^3A_2$ and ^3E levels was discussed in detail in [15,27]. Analysis of the integral intensities of the EPR signals $g_1 = 4.27$, obtained by the double integration method and related to the masses of the powders under study, indicates the concentration of fluorescent $NV^{(-)}$ centers in FND-1, FND-2 and FND-3 of the order of ~ 1.2, ~ 4 and 5.5 ppm. Thus, the EPR method can be used to independently estimate the concentration of $NV^{(-)}$ centers in fluorescent diamonds less than 100–150 nm in size, where these centers were specially created (by irradiation with high-energy electron beams).

Luminescence

The luminescence spectra of FND-1, FND-2, and FND-3 obtained upon excitation by laser radiation with wavelength of 532 nm exhibit characteristic broad bands associated with emission from $NV^{(-)}$ centers (Fig. 6, curves *1, 2* and *3*). The identity of the last two spectra was checked by their superposition and alignment using an adjustable scale factor. Both spectra (*2* and *3*) contain identical features marked by vertical dotted lines (Fig. 6). The material with the longest time of irradiation with high-energy electrons (FND-3) and the highest concentration of $NV^{(-)}$ centers exhibits a luminescence band within the range from 600 to 820 nm, including a narrow zero-phonon line at 637 nm and modulations in the range of 650–820 nm associated with phonon repetitions. The spectrum of this type almost completely coincides with the spectrum of fluorescent micron-sized synthetic diamond crystals obtained using the same irradiation technique [28]. We have found that the luminescence intensity of the FND-3 is excellent for any practical use as a sensor. A fluorescent image of a dried

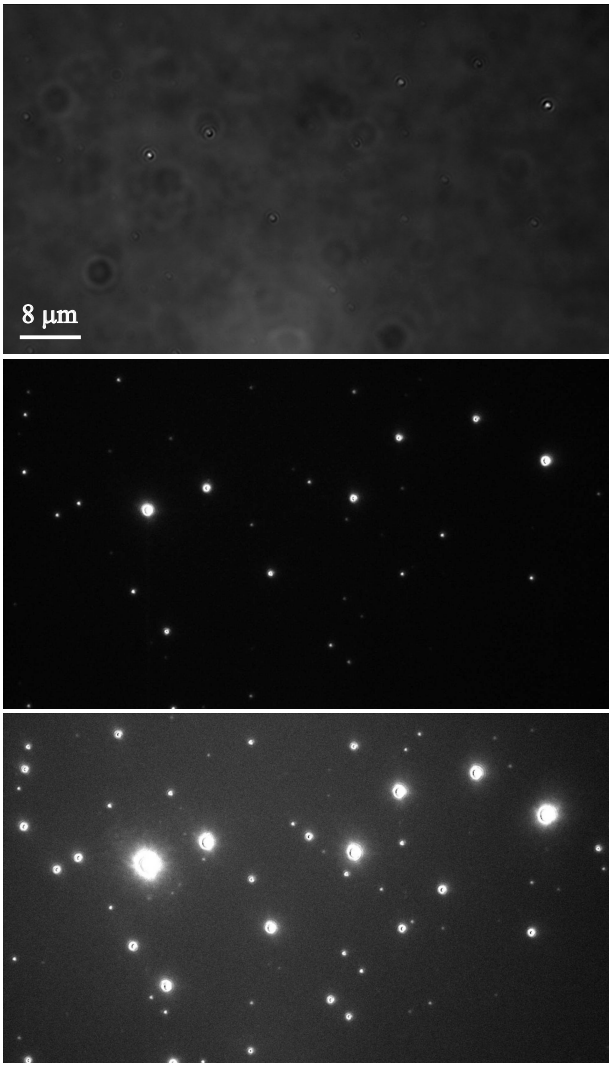

Figure 8. Optical and fluorescent images of isolated FND-2 particles on a glass substrate obtained using different optical microscopy methods: in differential interference contrast mode with white light irradiation (a), and when irradiated with exciting laser radiation at wavelength of 561 nm with image exposure times of 60 (b) and 600 ms (c).

drop of suspension of FND-3 nanoparticles, obtained using a filter that transmits radiation in the range of 600−660 nm, is shown in Fig. 7. It indicates the presence of more or less uniformly and brightly luminous regions inside the ring, the size of which is given by the diameter of the drop. Luminescence intensity of these regions is proportional to the concentration of the material deposited in them during drying of the suspension drop. Figure 8 shows images of isolated FND-2 particles and their aggregates deposited on the coverglass, obtained using a multifunctional microscope in the differential interference contrast mode when irradiated with white light (Fig. 8, a) , and in the fluorescence mode when irradiated with 561 nm radiation and exposure times of 60 and 600 ms (Fig. 8, b, c). With an increase in the frame exposure time up to 600 ms, more particles become visible, which have a smaller number of emission centers and do not appear at exposure of 60 ms. At the same time, in both fluorescence images (Fig. 8, b, c), small particles with low emission capacity are perfectly manifested, which, for fundamental reasons, can not be resolved in differential interference-contrast images, obtained in the transmission mode (Fig. 8, a). These particles have sizes less than 50 nm and, accordingly, a smaller number of emission $NV^{(-)}$ centers. In turn, the brightest spots in Fig. 8, b,c are most likely due to aggregates of three or four (or more) randomly agglutinated 100 nm particles. The excellent fluorescence characteristics of FND-3 are due to both the high concentration of $NV^{(-)}$ centers (5.5 ppm) and the high quality of the diamond lattice in crystallite particles with average size of 100 nm. The average photon flux detected from a single FND-3 fluorescent particle under the conditions of optical excitation used (in this article) is quite intense and is about $\sim (9-10) \cdot 10^6$ kcs/s. If we assume that only one $NV^{(-)}$ center leads to the detection of a quasi-stationary photon flux of ~ 20 kcs/s, as is the case for small particles with one center inside [1], then we get about $\sim 450-500$ $NV^{(-)}$ centers in one ~ 100 nm FND-3 particle. The estimates made based on luminescence intensity measurements are in good agreement with the those of the $NV^{(-)}$ concentration obtained from the analysis of the integral intensity of the EPR signal $g_1 = 4.27$. The total number of defects induced by grinding, both in the lattice itself and in the mechanically damaged region near the surface (up to 10−12 nm deep), is insignificant for quenching the luminescence of $NV^{(-)}$ centers inside such 100 nm particles, and can be controlled in advance by the method of electron paramagnetic resonance. Specially irradiated and annealed synthetic HPHT crystals of Ib diamond 100 nm in size can be used in micro-optical devices, fiber systems and sensors operating on nanophotonics principles. In terms of their characteristics, 100 nm FND studied in this article yield similar fluorescence intensity from the same excitation volume, compared to bulk diamond microcrystals with $NV^{(-)}$ centers. Such a fluorescence intensity is compatible with the requirements for organelle contouring and tracking of endosomal dynamics in a cell with FND [29,30]. Radiation from particles injected under the skin of experimental laboratory animals can also be detected by standard optical means.

Conclusion

Synthetic nanodiamonds with particle size of ~ 100 nm, irradiated in the submicron morphological state and then annealed, demonstrate high (up to 5.5 ppm) concentration of $NV^{(-)}$ centers simultaneously with the absence of a noticeable number of surface defects (multivacancies) induced by the initial mechanical grinding. The EPR spectrum recording of weak signals in half magnetic field is allows not only to estimate the concentration of $NV^{(-)}$ centers in synthetic HPHT Ib fluorescent nanodiamonds,

but also to asses the quality of the crystal lattice in the vicinity of $NV^{(-)}$ centers according to the shape of the saturation curves of the EPR signal amplitudes corresponding to the forbidden and allowed transitions in these triplet centers. EPR and fluorescence results indicate that the crystalline quality of the lattice in 100 nm particles of fluorescent diamond does not differ much from that for bulk diamond, and is quite acceptable for obtaining bright and superbright luminescence from such particles. The integral intensity of the EPR signal from $NV^{(-)}$ centers associated with forbidden transitions correlates with the luminescence intensity of $NV^{(-)}$ centers in 100 nm particles within the spectral range of 600–800 nm.

Acknowledgments

The authors thank prof. Kazuyuki Takai (Hosei University, Japan) for assistance in magnetic research. V.Yu.O. thanks the University Ecole Normale Supérieure de Paris-Saclay (Gif-sur-Yvette, France) for their support as a visiting professor and the opportunity to conduct experiments on the topic of this article.

Funding

This article was supported by the Russian Science Foundation (agreement 21-12-00264).

Conflict of interest

The authors declare that they have no conflict of interest within the scope of the study presented in this article.

References

[1] H.C. Chang, W.W.W. Hsiao, M.C. Su. *Fluorescent nanodiamonds.* (John Wiley & Sons, Hoboken-Chichester-Oxford, 2019).
[2] S.J. Yu, M.W. Kang, H.C. Chang, K.M. Chen, Y.C. Yu. J. Am. Chem. Soc., **127** (50), 17604 (2005). DOI: 10.1021/ja0567081
[3] R. Schirhagl, K. Chang, M. Loretz, C.L. Degen. Annu. Rev. Phys. Chem., **65**, 83 (2004). DOI: 10.1146/annurev-physchem-040513-103659
[4] O. Shenderova, G. McGuire. Biointerphases, **10**, 030802 (2015). DOI: 10.1116/1.4927679
[5] A.I. Shames, V.Y. Osipov, H.J. von Bardeleben, J.P. Boudou, F. Treussart, A.Y. Vul'. Appl. Phys. Lett., **104** (6), 063107 (2014). DOI: 10.1063/1.4865205
[6] A.I. Shames, V.Y. Osipov, J.P. Boudou, A.M. Panich, H.J. von Bardeleben, F. Treussart, A.Y. Vul'. J. Phys. D: Appl. Phys., **48** (15), 155302 (2015). DOI: 10.1088/0022-3727/48/15/155302
[7] J.H.N. Loubser, J.A. van Wyk. Rep. Prog. Phys., **41**, 1201 (1978). DOI: 10.1088/0034-4885/41/8/002
[8] A.M. Zaitsev *Optical properties of diamond: A data handbook.* (Springer–Verlag, Berlin–Heidelberg–New York, 2001). DOI: 10.1007/978-3-662-04548-0
[9] G. Davies, M.F. Hamer. Proc. R. Soc. Lond. A. Math. Phys. Sci., **348** (1653), 285 (1976). DOI: 10.1098/rspa.1976.0039
[10] V.Y. Osipov, F. Treussart, S.A. Zargaleh, K. Takai, F.M. Shakhov, B.T. Hogan, A. Baldycheva. Nanoscale Res. Lett., *14* (1), 1 (2019). DOI: 10.1186/s11671-019-3111-y
[11] G.K. Walters, T.L. Estle. J. Appl. Phys., **32**, 1854 (1961). DOI: 10.1063/1.1728252
[12] T. Rosskopf, A. Dussaux, K. Ohashi, M. Loretz, R. Schirhagl, H. Watanabe, S. Shikata, K.M. Itoh, C.L. Degen. Phys. Rev. Lett., **112**, 147602 (2014). DOI: 10.1103/PhysRevLett.112.147602
[13] D.W. Boukhvalov, V.Y. Osipov, K. Takai. Phys. Chem. Chem. Phys., **23**, 14592 (2021). DOI: 10.1039/D0CP05914E
[14] V.Y. Osipov, F.M. Shakhov, K.V. Bogdanov, K. Takai, T. Hayashi, F. Treussart, A. Baldycheva, B.T. Hogan, C. Jentgens. Nanoscale Res. Lett., **15** (1), 1 (2020). DOI: 10.1186/s11671-020-03433-7
[15] M.W. Doherty, V.V. Struzhkin, D.A. Simpson, L.P. McGuinness, Y. Meng, A. Stacey, T.J. Karle, R.J. Hemley, N.B. Manson, L.C.L. Hollenberg, S. Prawer. Phys. Rev. Lett., **112** (4), 047601 (2014). DOI: 10.1103/PhysRevLett.112.047601
[16] D.A. Broadway, B.C. Johnson, M.S.J. Barson, S.E. Lillie, N. Dontschuk, D.J. McCloskey, A. Tsai, T. Teraji, D.A. Simpson, A. Stacey, J.C. McCallum, J.E. Bradby, M.W. Doherty, L.C.L. Hollenberg, J.-P. Tetienne. Nano Lett., **19** (7), 4543 (2019). DOI: 10.1021/acs.nanolett.9b01402
[17] V.Y. Osipov, F.M. Shakhov, N.N. Efimov, V.V. Minin, S.V. Kidalov, A.Y. Vul'. Solid State Phys., **59** (6), 1146 (2017). DOI: 10.1134/S1063783417060191
[18] W.V. Smith, P.P. Sorokin, I.L. Gelles, G.J. Lasher. Phys. Rev., **115**, 1546 (1959). DOI: 10.1103/PhysRev.115.1546
[19] B.R. Smith, D.W. Inglis, B. Sandnes, J.R. Rabeau, A.V. Zvyagin, D. Gruber, C.J. Noble, R. Vogel, E. Osawa, T. Plakhotnik. Small, **5**, 1649 (2009). DOI: 10.1002/smll.200801802
[20] V.Y. Osipov, A.I. Shames, T. Enoki, K. Takai, M.V. Baidakova, A.Y. Vul'. Diam. Relat. Mat., **16** (12), 2035 (2007). DOI: 10.1016/j.diamond.2007.06.003
[21] S. Sotoma, D. Terada, T.F. Segawa, R. Igarashi, Y. Harada, M. Shirakawa. Sci. Rep., **8** (1), 1 (2018). DOI: 10.1038/s41598-018-23635-5
[22] Á Gali. Nanophotonics, **8** (11), 1907 (2019). DOI: 10.1515/nanoph-2019-0154
[23] S.D. Subedi, V.V. Fedorov, J. Peppers, D.V. Martyshkin, S.B. Mirov, L. Shao, M. Loncar. Opt. Mater. Express, **9** (5), 2076 (2019). DOI: 10.1364/OME.9.002076
[24] M.W. Doherty, N.B. Manson, P. Delaney, F. Jelezko, J. Wrachtrup, L.C.L Hollenberg. Phys. Rep., **528** (1), 1 (2013). DOI: 10.1016/j.physrep.2013.02.001
[25] A.I. Shames, V.Y. Osipov, H.J. von Bardeleben, A.Y. Vul'. J. Phys.: Condens. Matter., **24** (22), 225302 (2012). DOI: 10.1088/0953-8984/24/22/225302
[26] S. Felton, A.M. Edmonds, M.E. Newton, P.M. Martineau, D. Fisher, D.J. Twitchen, J.M. Baker. Phys. Rev. B., **79** (7), 075203 (2009). DOI: 10.1103/PhysRevB.79.075203
[27] M.W. Doherty, N.B. Manson, P. Delaney, L.C.L. Hollenberg. New J. Phys., **13** (2), 025019 (2011). DOI: 10.1088/1367-2630/13/2/025019
[28] A.I. Shames, V.Y. Osipov, K.V. Bogdanov, A.V. Baranov, M.V. Zhukovskaya, A. Dalis, S.S. Vagarali, A. Rampersaud. J. Phys. Chem. C., **121** (9), 5232 (2017). DOI: 10.1021/acs.jpcc.6b12827

[29] I. Rehor, J. Slegerova, J. Kucka, V. Proks, V. Petrakova, M.-P. Adam, F. Treussart, S. Turner, S. Bals, P. Sacha, M. Ledvina, A.M. Wen, N.F. Steinmetz, P. Cigler. Small, **10** (6), 1106 (2014). DOI: 10.1002/smll.201302336

[30] S. Haziza, N. Mohan, Y. Loe-Mie, A.M. Lepagnol-Bestel, S. Massou, M.P. Adam, X.L. Le, J. Viard, C. Plancon, R. Daudin, P. Koebel, E. Dorard, C. Rose, F.-J. Hsieh, C.-C. Wu, B. Potier, Y. Herault, C. Sala, A. Corvin, B. Allinquant, H.-C. Chang, F. Treussart, M. Simonneau. Nat. Nanotechnol., **12** (4), 322 (2017). DOI: 10.1038/nnano.2016.260